Numerical Simulation of Random Packing of Spherical Particles for Powder-Based Additive Manufacturing

Jianhua Zhou
Mem. ASME

Yuwen Zhang[1]
Fellow ASME
e-mail: zhangyu@missouri.edu

J. K. Chen
Fellow ASME

Department of Mechanical and Aerospace Engineering,
University of Missouri,
Columbia, MO 65211

Powder-based additive manufacturing is an efficient and rapid manufacturing technique because it allows fabrication of complex parts that are often unobtainable by traditional manufacturing processes. A better understanding of the packing structure of the powder is urgently needed for the powder-based additive manufacturing. In this study, the sequential addition packing algorithm is employed to investigate the random packing of spherical particles with and without shaking effect. The 3D random packing structures are demonstrated by illustrative pictures and quantified in terms of pair distribution function, coordination number, and packing density. The results are presented and discussed aiming to produce the desirable packing structures for powder-based additive manufacturing. [DOI: 10.1115/1.3123324]

1 Introduction

Powder-based additive manufacturing, including selective laser sintering (SLS), is an emerging technology that can fabricate structurally-sound parts from powdered material using a directed laser beam [1]. It is an efficient and rapid manufacturing technique because it allows for the manufacture of complex parts that are often unobtainable by other conventional manufacturing processes [2,3]. One obstacle of the SLS process is the balling phenomenon, in which melted powder grains stick to each other via surface tension forces, thereby forming a series of spheres with diameters approximately equal to the diameter of the laser beam [2,4]. One way to overcome the balling phenomenon is to use a powder bed consisting of two different types of metal powders, one with a significantly higher melting point than the other as suggested by Bunnell [5]. During the SLS process, only powder particles with lower melting point will be molten and the high-melting point powder particles will remain solid all the time.

The balling phenomena can also be overcome by using bimodal powders that contain mixture of powder particles of the same composition but with two distinctive sizes. When mixture of powder particles of the same composition but different sizes is irradiated by a laser beam, responses of the particles will be different depending on their sizes. Our preliminary work [6] has shown that the increase in the surface temperature of the smaller particles will be faster than the large particles because the thermal inertia of the smaller particle is lower. This will lead to the complete melting of the smaller particles in the mixture while the large particle is still solid. The different responses of particles with different sizes allow us to use small particles as binder to bind large particles (of the same or different kinds) to form functional parts. Thus, it is indispensable to investigate the structural details via packing algorithms or experiments with binary size distribution.

Random packing of spheres with constant or different diameters plays an important role in many branches of physics and engineering [7,8]. In the past, experimental investigations (e.g., Refs. [9,10]) and computer simulations (e.g., Refs. [11–15]) were intensively carried out to study the random packing of particles. Though experiments are important means to obtain many packing properties, it is very difficult, if not impossible, to provide some important details on packing structures, e.g., the coordination number of each particle in the packing bed. Therefore, it is necessary to use numerical simulation to investigate those details. There are various particle packing algorithms. Generally speaking, the existing packing simulation techniques can be grouped into three types: (1) sequential addition, (2) nonsequential rearrangement, and (3) dynamic simulation. The first algorithm simulates the successive packing of particles in a container with particles dropping one by one in the gravitational field [11,15,16]. A sphere that has three contacts with earlier packed spheres is considered to be in its final position if it is stable. The sequential addition method describes the actual process of packing generation in experiments without considering interacted forces among particles and vibration. The second algorithm starts with a very dense configuration of large spheres, which can even overlap [12–14]. It then moves the spheres in order to reduce the degree of overlapping. The third algorithm is based on the discrete element method (DEM) [17]. It treats particle packing as a dynamic process where interparticle forces are explicitly considered.

In this study, the sequential addition algorithm is employed to simulate the random packing process of spherical particles with two different size distributions (monosize distribution and bimodal distribution). This packing algorithm is chosen as the numerical method just because of its simplicity and ease in programming and running on a PC. The influence of the shaking effect on the packing structure is examined in detail. Our attention is focused on the applications of the packing simulation method in the powder-based manufacturing process. Packing parameters suitable for powder-based additive manufacturing are obtained and recommended to guide the laser sintering process.

2 Computational Method

The sequential addition packing simulation starts with randomly choosing a sphere according to a pregenerated particle size distribution and then dropping the sphere into a rectangular container with a dimension $x_{max} \times y_{max} \times z_{max}$. The final positions of the incoming spheres are obtained by using the dropping and rolling rules, which are devised from a similar physical process of spheres dropping in the gravitational field to minimize its gravity potential. Initially, the sphere is given a coordinate of (x, y, z), where (x, y) is chosen randomly and z is well above the top of the

[1]Corresponding author.

Contributed by the Manufacturing Engineering Division of ASME for publication in the JOURNAL OF MANUFACTURING SCIENCE AND ENGINEERING. Manuscript received February 14, 2008; final manuscript received March 28, 2009; published online April 30, 2009. Review conducted by Shaochen Chen.

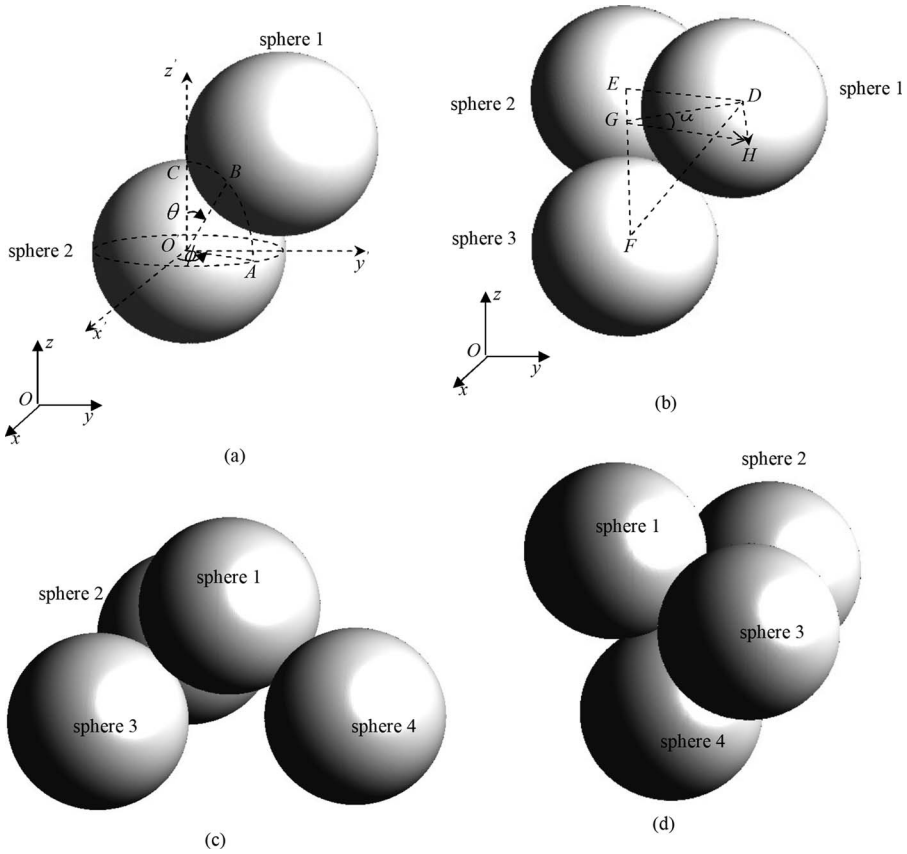

Fig. 1 Several geometrical configurations during the rolling of spheres: (*a*) incoming sphere is rolling down on one sphere, (*b*) incoming sphere is rolling down on two spheres, (*c*) incoming sphere is supported by three spheres and the support is stable, and (*d*) incoming sphere is supported by three spheres but the support is unstable

defined container. Each sphere moves down along a vertical path (i.e., constants x and y with varying z) until its surface contacts the floor of the container or a deposited sphere. If it contacts the floor, its final position will be determined. If not, the rolling rules will be employed.

Figure 1 shows several geometrical configurations, which may be encountered during the sphere rolling process. In this figure, sphere 1 represents the incoming sphere, and spheres 2, 3, and 4 denote the spheres deposited earlier. A global Cartesian coordinate system (x,y,z) is used to describe the position of each sphere in the container. Figure 1(a) depicts the case where the incoming sphere 1 is rolling down in a vertical plane on sphere 2. For this case, the rolling algorithm can be implemented by establishing a local spherical coordinate system (x',y',z') whose origin coincides with the center of sphere 2 and the three axes are parallel to the x, y, and z axes, respectively. With this local spherical coordinate system, the position of sphere 1 can be specified in terms of the radii of the two contacting spheres and the zenith and azimuth angles (θ and ϕ, respectively) as follows:

$$x_1 = x_2 + (r_1 + r_2) \cdot \cos\,\theta \cdot \cos\,\phi \tag{1}$$

$$y_1 = y_2 + (r_1 + r_2) \cdot \cos\,\theta \cdot \sin\,\phi \tag{2}$$

$$z_1 = z_2 + (r_1 + r_2) \cdot \sin\,\theta \tag{3}$$

where (x_1,y_1,z_1) and (x_2,y_2,z_2) are the center positions of the two spheres in the global coordinate system, r_1 and r_2 are their radii, and the zenith angle θ is measured from $+z'$ to the line connecting the two centroids of the spheres.

The rolling of sphere 1 on sphere 2 in a vertical plane is realized by the change in the zenith angle θ. If the change in the angle $\delta\theta$ is small, the new position of sphere 1 can be calculated as

$$x_1 = x_2 + (r_1 + r_2) \cdot \cos(\theta + \delta\theta) \cdot \cos\,\phi \tag{4}$$

$$y_1 = y_2 + (r_1 + r_2) \cdot \cos(\theta + \delta\theta) \cdot \sin\,\phi \tag{5}$$

$$z_1 = z_2 + (r_1 + r_2) \cdot \sin(\theta + \delta\theta) \tag{6}$$

Sphere 1 keeps rolling down on sphere 2 in the vertical plane until it hits another sphere 3. However, a sphere in contact with only two spheres is unstable. Therefore, sphere 1 will continue to roll down while keeping in touch with the two spheres (spheres 2 and 3). This is illustrated in Fig. 1(b). For this case, the rolling of sphere 1 can be simulated by vector operations. In the following derivations, the symbol $\boldsymbol{EF}$ denotes the vector joining the centers of the spheres 2 and 3 (E and F are the centers of sphere 2 and 3, respectively). The direction of $\boldsymbol{EF}$ is from E to F. Other vectors can be understood in a similar way and will not be explained. The centers of the three spheres define a plane DEF. The line segment DG is perpendicular to $\boldsymbol{EF}$. The position of point G can be determined by the scalar product of vectors $\boldsymbol{ED}$ and $\boldsymbol{EF}$ as follows:

$$\boldsymbol{OG} = \boldsymbol{OE} + \boldsymbol{EF}\frac{\boldsymbol{ED} \cdot \boldsymbol{EF}}{|\boldsymbol{EF}|^2} \tag{7}$$

where O is the origin of the global Cartesian coordinate system (x,y,z), and $|\boldsymbol{EF}|$ denotes the magnitude of the vector $\boldsymbol{EF}$.

As the sphere 1 rolls, the path of its center is a circular arc whose radius is $|\boldsymbol{GD}|$. This rolling path lies in the plane with its

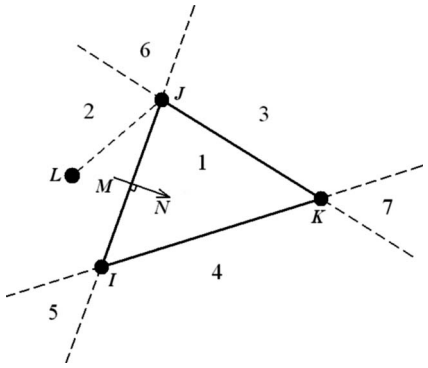

Fig. 2 Stabilization judgment when the incoming sphere is in contact with three spheres deposited earlier

normal along the vector ***EF***. In Fig. 1(*b*), ***DH*** denotes the vector that is perpendicular to the plane *DEF* and tangent to the circumference of the rolling circle of sphere 1. The vector ***DH*** can be calculated by the vector product of ***GD*** and ***EF***. Thus, vector ***GH*** after rolling a small angle α is evaluated as follows:

$$\boldsymbol{GH} = \boldsymbol{GD} + \boldsymbol{DH} = \boldsymbol{GD} + \frac{\boldsymbol{GD} \times \boldsymbol{EF}}{|\boldsymbol{GD} \times \boldsymbol{EF}|} |\boldsymbol{GD}| \tan \alpha \tag{8}$$

The new position H (i.e., vector ***OH***) can then be computed by

$$\boldsymbol{OH} = \boldsymbol{OG} + \frac{\boldsymbol{GH}}{|\boldsymbol{GH}|} |\boldsymbol{GD}| \tag{9}$$

To ensure the rolling path of point D is a circular arc, the magnitude of vector ***GH*** is normalized to $|\boldsymbol{GD}|$ through the second term at the right hand side of Eq. (9).

Sphere 1 rolls downwards in contact with spheres 2 and 3 until it hits another one (say sphere 4). Once it happens, a stabilization judgment will be performed to ensure that the incoming sphere (sphere 1) is in a stable position based on the criterion of minimum gravitational potential. Figures 1(*c*) and 1(*d*) show the two cases where the incoming sphere is in contact with three spheres. The difference between Figs. 1(*c*) and 1(*d*) is that the former is a stable configuration while the latter is an unstable one. In the following, the stabilization judgment will be addressed with the aid of Fig. 2.

Figure 2 shows a top view (i.e., the projection on the horizontal plane *x*-*o*-*y*) of the geometrical configuration where the incoming sphere 1 (its center projection on the plane is point L) is in contact with other three spheres (their center projections on the plane are points I, J, and K, respectively). If point L is enclosed in the triangle ΔIJK, then the incoming sphere is stable. If point L is outside the triangle, then the incoming sphere is unstable. At first thought, the mathematics seems to be complicated for the stabilization judgment, but a more detailed inspection indicates that the stabilization judgment can be converted to a basic question, i.e., "Is point L on the same side (with respect to the line IJ) as the point K?" Thus, the problem can simply be resolved using the following approach.

Let ***MN*** be a vector that is obtained by a 90 deg rotation in the clockwise direction from vector ***IJ***, see Fig. 2. The vector ***IJ*** can be expressed with its three components as $(x_J - x_I, y_J - y_I, 0)$. Thus, the vector ***MN*** is written as $(y_J - y_I, x_I - x_J, 0)$. The scalar product of ***MN*** and ***JK*** is

$$a = (x_K - x_J)(y_J - y_I) + (y_K - y_J)(x_I - x_J) \tag{10}$$

and the scalar product of ***MN*** and ***JL*** is

$$b = (x_L - x_J)(y_J - y_I) + (y_L - y_J)(x_I - x_J) \tag{11}$$

If $ab > 0$, the points L and K are on the same side of the line IJ; otherwise, they are on the opposite sides.

The locations of L with respect to other two lines JK and KI can be judged by using a similar method. The final location (i.e., in one of the regions 1–7 in Fig. 2) of the point L is determined according to the combination of the above-mentioned judgment algorithms.

If an incoming sphere is stable (i.e., point L is in the domain 1 in Fig. 2), its final location is determined and the computer program will turn to generate a new sphere. Otherwise, the sphere continues to roll down on two other spheres or one sphere. For example, if point L is found to be in the domain 2, the incoming sphere L will roll on spheres I and J; if L is in the domain 6, it will roll on the sphere J. Anytime when a falling sphere reaches the bottom of the container, the sphere stops and a new sphere will be generated and traced.

Figure 3 shows the program flow chart. In addition, an appropriate boundary of the container should be considered to eliminate the wall effects [15,16]. In this paper, the periodic boundaries are applied to resolve the problem of wall effects as in our previous work [18]. By using these boundaries, any sphere that leaves the container through one of its four surrounding vertical walls or corners will immediately re-enter the opposite wall or corner.

In the above-mentioned simulation procedure, the packing structure is built up by dropping a single sphere at each addition step. A higher packing density can be achieved by shaking the container. Following the shaking algorithm [11], we drop l trial spheres at each addition step, but only the one whose final position is lowest is retained and becomes a permanent part of the packing bed. After introducing the shaking algorithm, small spheres may fill the empty space between large spheres and thus make the packing structure denser.

3 Results and Discussions

The parameters that describe the quality of a packing structure include packing density and coordination number. The packing density is defined as the total volume of spheres divided by the volume of box taken by these spheres. The coordination number is the number of spheres in contact with any given sphere. The average coordination number is defined as the summation of the coordination number of each sphere divides the total number of the spheres N_t. These parameters will be computed in the following numerical analysis.

Packing of monosized particles are simulated first because it is helpful to validate the present model. It can also be used to determine the dimensions of the packing container that can give dimension-independent results. Figure 4 shows the packing density and the average coordination number as functions of container dimensions. In this simulation, the container dimensions in the x and y directions are the same and the radius of the sphere is set as the unit of the dimensions. As can be seen from Figs. 4(*a*) and 4(*b*), both the packing density and the average coordination number increase with increasing container height (i.e., the dimension in the z direction, $z_{\max}$). However, it is noticed that as the container height increases to about 50, the packing density and average coordination number tend to be saturated. It is observed from Figs. 4(*c*) and 4(*d*) that the packing density and average coordination number almost keep constant as the container dimension in the x- or y-direction increase (the container dimension in the z-direction remains at the value of 50). This can be ascribed to the application of the periodic boundary condition in the x- and y-directions. Our simulation shows that for monosized loose packing, the stable packing density is about 0.578, and the average coordination number is about 5.915. Both agree well with the reported values in the literatures (e.g., Ref. [15]). Therefore, the dimensions of $20 \times 20 \times 50$ will be employed for the rest of the simulation cases of the random sphere packing.

Figure 5 shows the 3D packing structure and the 2D cross-sectional view at the midplane $y = 0.5 y_{\max}$ for the monosized particle packing. Circles with different radii are observed on the 2D cross-sectional view. This is because the random packing spheres

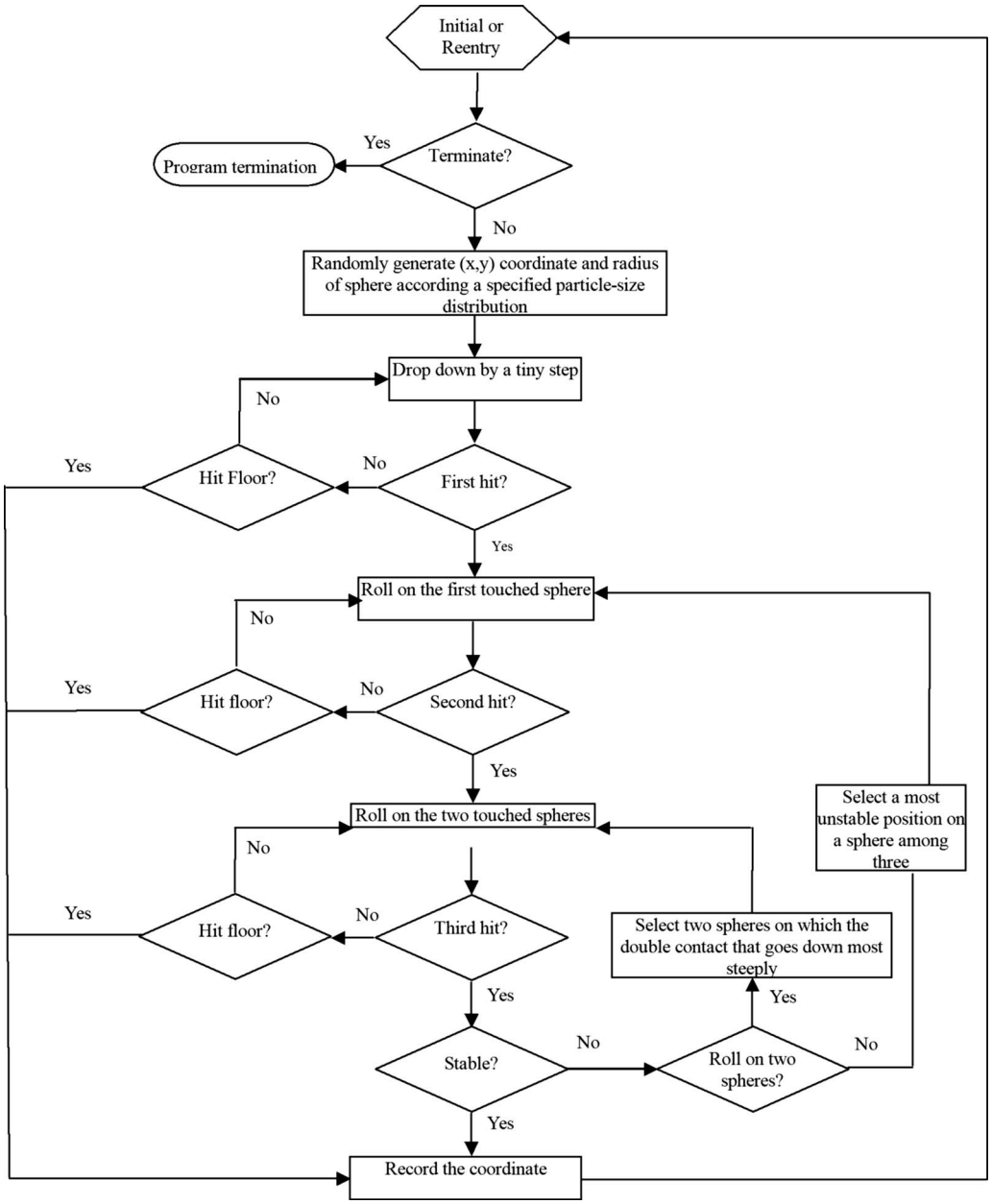

Fig. 3 Flowchart of the sequential addition algorithm

cut by the vertical plane are at many different distances from that plane. It can be seen from Fig. 5 that the packing structure for the bimodal size distribution has a good randomicity, and no ordered domains are found throughout the packing structure.

The balling phenomenon in SLS is a serious obstacle that results in low part-quality. One way to overcome the balling phenomenon in SLS is to use a powder bed consisting of two different types of metal powders. Besides the physical properties of different types of metal powders, the structure of the powder bed that is composed by two different sizes of particles is also critical to ensure high quality of the sintered parts. For this application, one can assume a bimodal distribution for the packing simulation, meaning that there are particles with two distinctive radii in the packing bed.

Figure 6 shows the 3D packing structure and the 2D cross-sectional view at the midplane $y=0.5y_{\max}$ for the bimodal distribution packing. In this case, the population ratio of the large spheres to the small spheres is $n_1/n_2=5:5$ and the radius ratio of the large spheres to the small spheres is $r_1/r_2=2:1$. The radius of the small sphere is set at the unit of the dimension. The obtained packing density and average coordination number are 0.591 and 5.773, respectively. Compared with the monosized packing, the packing density is increased whereas the average coordination number is decreased. This is mainly attributed to the decreasing average number on small-size spheres, as can be seen from the following structural analyses.

For SLS process, higher packing density is generally desirable. Our simulations showed that, after introducing the shaking effect, the packing density and average coordination number increase to 0.589 and 5.939, respectively, for the monosized packing and 0.617 and 5.774, respectively, for the bimodal packing ($n_1/n_2=5:5$, $r_1/r_2=2:1$).

More numerical experiments are made for different mixture compositions with or without the shaking effects. Table 1 summarizes the calculating results for these simulations. It can be seen that except for the case of $n_1/n_2=6:4$ (which means the number of large spheres is larger than that of the small spheres), both the

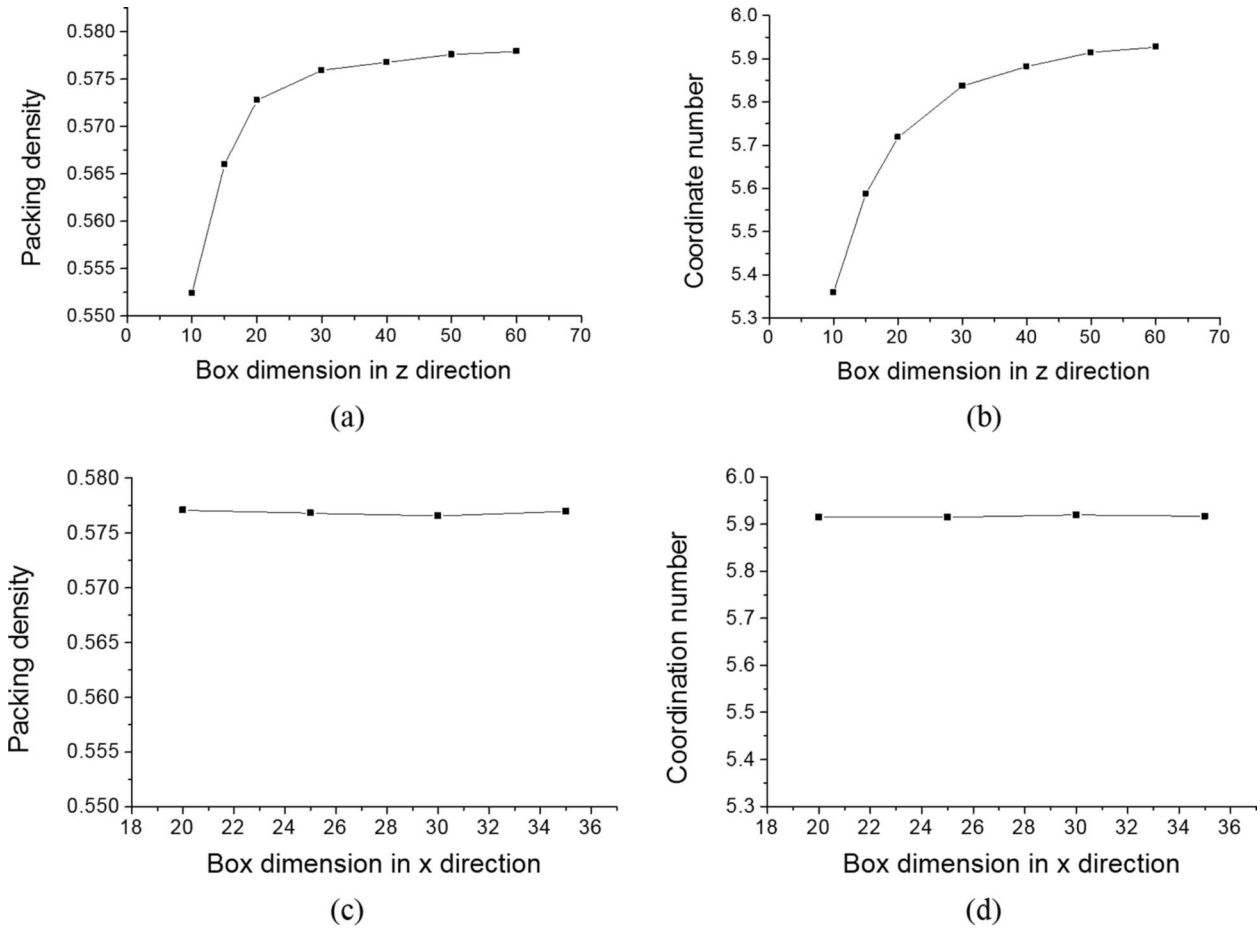

Fig. 4 Packing density and coordination number for monosized packing

packing density and average coordination number can be increased via the shaking algorithm. It is also found that both the packing density and the average coordination number for the case $n_1/n_2=4:6$ are higher than those for the case $n_1/n_2=4:6$. Therefore, the case $n_1/n_2=6:4$ should be avoided in the SLS process because a low coordination number results in loose contacts of particles during sintering, which, in turn, causes some structural defects such as lower stiffness and weak strength of the fabricated parts.

The following discussions will be based on the packing simulations with the shaking effect. The number of trial spheres at each addition step is $l=4$ as suggested in Ref. [11]. Figure 7 gives the distribution of the contact number per particle (i.e., coordination number) for the bimodal packing ($n_1/n_2=5:5$, $r_1/r_2=2:1$). The vertical coordination variable "Fraction" in Fig. 7 means that the ratio of the number of spheres whose coordination number is at a certain value to the total simulation sphere number N_t. It can be found in Fig. 7 that for the bimodal packing, there are two peaks of the number of the contacted particles. The first peak takes place at the coordination number 4, which corresponds to the coordination number for the smaller spheres. The second peak happens at the coordination number 8, which corresponds to the coordination number for the larger spheres. They can be explained as follows. Larger spheres have higher coordination numbers because small spheres exclude less area on the surface of the larger spheres than spheres of equal size do. However, large spheres prevent adjacent small spheres from contacting with more spheres, leading to a low coordination number for the smaller spheres. On the other hand, there is only one peak at the coordination number of 6 for the monosized case as seen in Fig. 7.

Another parameter, the pair distribution function $g(r)$ is also widely used to characterize the random packing structure as it contains useful information about interparticle radial correlations [19]. The pair distribution function $g(r)$ is usually defined as follows:

$$g(r) = \frac{dN}{N_t \cdot r \cdot dr} \tag{12}$$

where dN is the number of pairs of spheres, the centers of which are separated by distances in the interval $(r, r+dr)$; and N_t is the total number of spheres. Figure 8 shows the pair distribution function for bimodal packing. The radius of the smaller spheres is set as the unit of the dimension. There are three peaks occurring at $r=2$, 3, and 4. Among them, the second peak that occurs at $r=3$ is the highest, which means the contacts between large spheres (radius=2) and small spheres (radius=1) constitute the main type of particle connection in the powder bed.

Figure 9 shows the effects of different population ratios on the coordination number distribution and the pair distribution function. It can be seen from Fig. 9(*a*) that the fraction of the spheres whose coordination number is 8 increases with increasing population of the larger spheres, and the fraction of the spheres whose coordination number is 4 drops as the population of smaller spheres decreases. Figures 9(*b*) and 9(*c*) indicate that when the number of larger spheres is less than that of the smaller spheres (i.e., the case of $n_1/n_2=4:6$), most of the structures in the powder bed is of a large-small sphere connection type (the peak value at $r=3$ is much lager than those at $r=2$ and 4.) However, when the number of larger spheres is greater than that of the smaller spheres

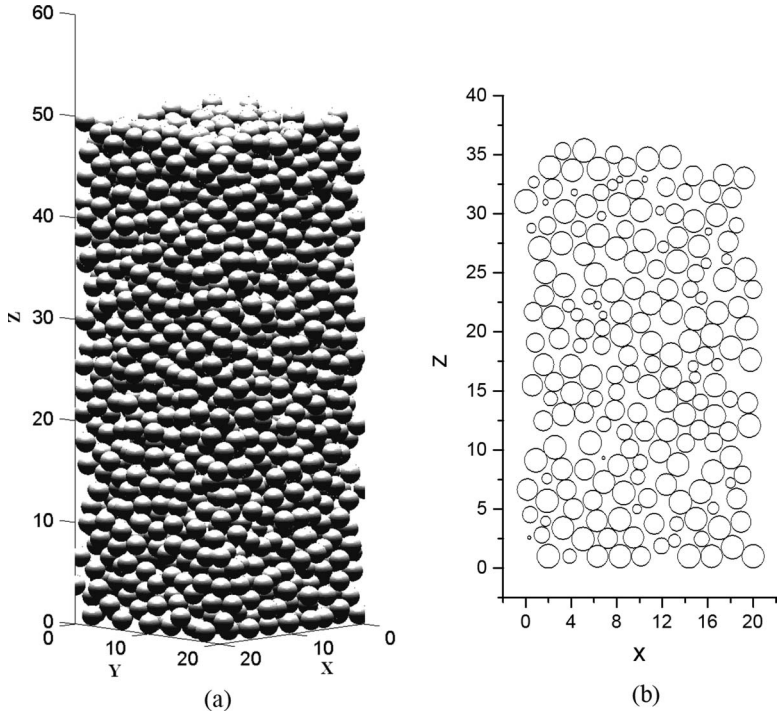

Fig. 5 Packing structure for equal size distribution: (*a*) 3D view, (*b*) 2D cross-sectional view at the plane $y=0.5y_{max}$

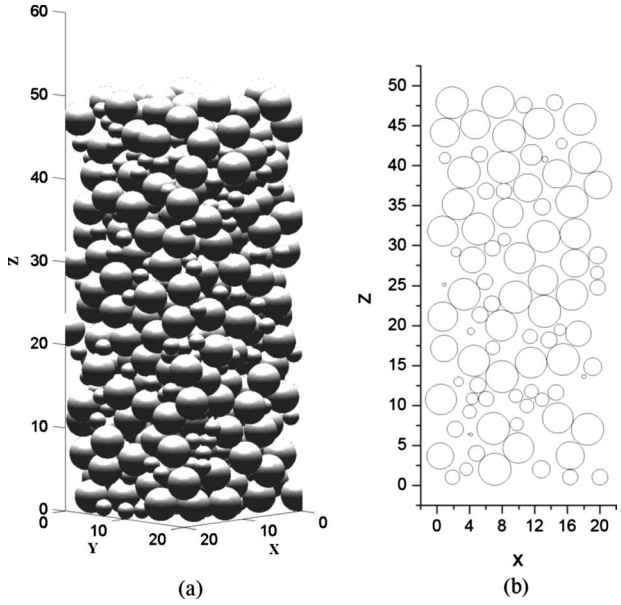

Fig. 6 Packing structure for bimodal size distribution: (*a*) 3D view, (*b*) 2D cross-sectional view at the plane $y=0.5y_{max}$

(i.e., the case of $n_1/n_2=6:4$), the number of large-large sphere connections becomes comparable to that of the large-small particle connections (i.e., the peak values at $r=3$ and $r=4$ are close to each other while the peak value at $r=2$ is much smaller)

4 Conclusions

The sequential addition packing algorithm is employed to simulate the random packing process of spherical particles. The numerical model is then used to investigate the random packing of spherical particles with and without the shaking effect. The results are particularly analyzed for the SLS manufacturing process aiming to produce the optimal packing parameters. It is found that to obtain high quality parts, a bimodal distribution where the number of large particles is less than that of the small particles is recommended since both the packing density and the coordination number can be increased for this case. Some important details about the packing structures are successfully obtained via the numerical algorithm developed in this study. It is shown that, compared with monosized packing, the packing density of bimodal packing is increased whereas the average coordination number is decreased. The fraction distribution of the coordination number and the pair distribution function are also used to characterize different packing structures. It is found that for monosized packing, there is only one peak (which happens at the coordination number 6) in the fraction distribution curve of the coordination number. However, there are two peaks in the fraction distribution curve for the bi-

Table 1 Comparison of simulation results with and without shaking effect for different population ratios of spheres ($r_1/r_2=2:1$)

	$n_1/n_2=4:6$		$n_1/n_2=5:5$		$n_1/n_2=6:4$	
	Coordination No.	Packing density	Coordination No.	Packing density	Coordination No.	Packing density
Without shaking effect	5.770	0.594	5.773	0.591	5.746	0.573
With shaking effect	5.779	0.615	5.774	0.617	5.725	0.613

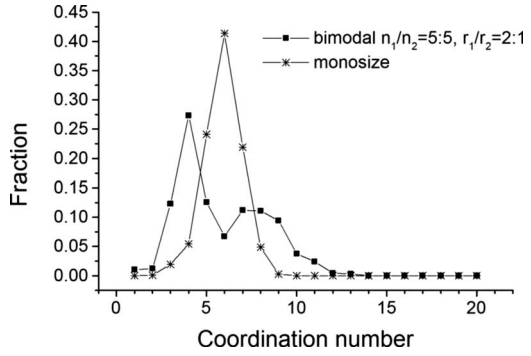

Fig. 7 Distribution of the coordination number per particle

modal packing. The first peak takes place at the coordination number 4, which corresponds to the coordination number for the smaller spheres. The second peak happens at the coordination number 8, which corresponds to the coordination number for the larger spheres. Further numerical experiments are performed to examine the effects of different population ratios on the coordination number distribution and the pair distribution function. It is revealed that the fraction of the spheres whose coordination number is 8 increases with increasing population of the larger spheres, and the fraction of the spheres whose coordination number is 4 drops as the population of smaller spheres decreases.

In the SLS processes, the three-dimensional functional parts are created using the layered manufacturing technique by fusing powered materials with a moving laser beam. Melting and resolidification are the mechanisms that bond metal powder particles to form a layer and also bond different layers together to form a functional part. For reaching a desired sintering depth, heat transfer analysis needs to be performed such that laser parameters, such as laser intensity, laser beam radius, laser beam scanning velocity, etc., can be correctly chosen prior to the real SLS procedure. The theoretical model and numerical algorithm formulated in this study are not only critical to understanding the structural essentials in the SLS power beds but also provides a solid foundation aiming at establishing a powerful particle-level heat transfer model for the SLS process.

Acknowledgment

Support for this work by the U.S. National Science Foundation under Grant No. CBET-0730143 is gratefully acknowledged.

Nomenclature

a, b = temporary variables
$g(r)$ = pair distribution function

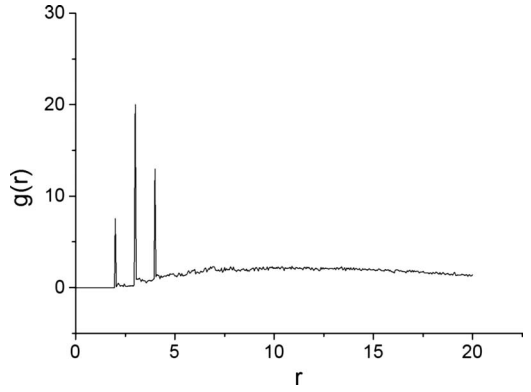

Fig. 8 Pair distribution function for bimodal distribution packing

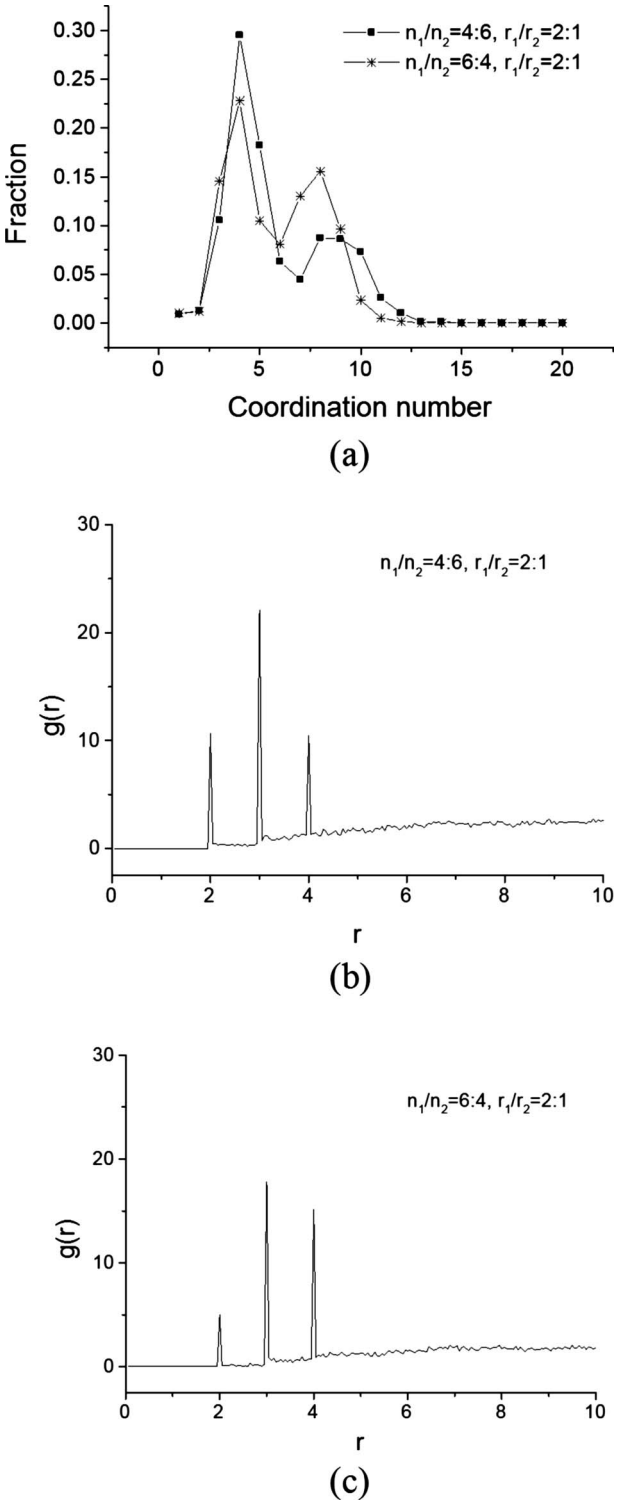

Fig. 9 Effects of different population ratios (n_1/n_2) on the coordination number distribution and pair distribution function

l = number of trial spheres in the shaking algorithm
n_1, n_2 = numbers of large-size spheres and small-size spheres, respectively
N_t = total simulation number of spheres
r = radius of sphere, m
x, y, z = overall Cartesian coordinate variables, m
x', y', z' = local Cartesian coordinate variables, m

x_{max}, y_{max}, z_{max} = the dimension of the packing container, m

Greek Symbols

θ = zenith angle, rad

ϕ = azimuth angle, rad

$\delta\theta$ = small change of zenith angle θ for rolling down calculation, rad

References

[1] Kruth, J.-P., 1995, "Rapid Prototyping—A New Application of Physical and Chemical Process for Material Accretion Manufacturing," *Proceedings of the 11th International Symposium for Electromachining*, Lausanne, pp. 3–28.

[2] Agarwala, M., Bourell, D., Beaman, J., Marcus, H., and Barlow, J., 1995, "Direct Selective Laser Sintering of Metals," Rapid Prototyping J., **1**, pp. 26–36.

[3] Das, S., Beaman, J., Wohlert, M., and Bourell, D., 1998, "Direct Laser Freeform Fabrication of High Performance Metal Components," Rapid Prototyping J., **4**, pp. 112–117.

[4] Tolochko, N. K., Mozzharov, S. E., Yadroitsev, I. A., Laoui, T., Froyen, L., Titov, V. I., and Ignatiev, M. B., 2004, "Balling Processes During Selective Laser Treatment of Powders," Rapid Prototyping J., **10**, pp. 78–87.

[5] Bunnell, D. E., 1995, "Fundamentals of Selective Laser Sintering of Metals," Ph.D. thesis, University of Texas at Austin, Austin, TX.

[6] Konrad, C., Zhang, Y., and Shi, Y., 2007, "Melting and Resolidification of Subcooled Metal Powder Particle Subjected to Nanosecond Laser Heating," Int. J. Heat Mass Transfer, **50**(11–12), pp. 2236–2245.

[7] Gray, W. A., 1969, *The Packing of Solid Particles*, Chapman and Hall, London.

[8] German, R. M., 1989, *Particle Packing Characteristics*, Metal Powder Industries Federation, Princeton, NJ.

[9] Scott, G. D., and Kilgour, D. M., 1969, "The Density of Random Close Packing of Spheres," J. Appl. Phys., J. Phys. D, **2**, pp. 863–866.

[10] Finney, J. L., 1970, "Random Packings and the Structure of Simple Liquids. I. The Geometry of Random Close Packing," Proc. R. Soc. London, Ser. A, **319**, pp. 479–493.

[11] Visscher, W. M., and Bolsterli, M., 1972, "Random Packing of Equal and Unequal Spheres in Two and Three Dimensions," Nature (London), **239**, pp. 504–507.

[12] Moscinski, J., Bargie, M., Rycerz, Z. A., and Jacobs, P. W. M., 1989, "The Force-Biased Algorithm for the Irregular Close Packing of Equal Hard Spheres," Mol. Simul., **3**, pp. 201–212.

[13] Jodrey, W. S., and Tory, E. M., 1981, "Computer Simulation of Isotropic, Homogeneous, Dense Random Packing of Equal Spheres," Powder Technol., **30**, pp. 111–118.

[14] Jodrey, W. S., and Tory, E. M., 1985, "Computer Simulation of Close Random Packing of Equal Spheres," Phys. Rev. A, **32**, pp. 2347–2351.

[15] Tory, E. M., Church, B. H., Tam, M. K., and Ratner, M., 1973, "Simulated Random Packing of Equal Spheres," Can. J. Chem. Eng., **51**, pp. 484–493.

[16] Jodrey, W. S., and Tory, E. M., 1979, "Simulation of Random Packing of Spheres," Simulation, **32**, pp. 1–12.

[17] Cundall, P. A., and Stack, O. D. L., 1979, "A Discrete Numerical Model for Granular Assemblies," Geotechnique, **29**(1), pp. 47–65.

[18] Y. Shi, and Y. Zhang, 2008, "Simulation of Random Packing of Spherical Particles With Different Size Distributions," Appl. Phys. A: Mater. Sci. Process., **92**(3), pp. 621–626.

[19] Dickinson, E., Milne, S. J., and Patel, M., 1989, "Ordering in Simulated Packed Beds Formed From Binary Mixtures of Particles in Two Dimensions: Implications for Ceramic Processing," Powder Technol., **59**, pp. 11–24.